

RESEARCH

Open Access



# Quantifying the fragmentation of polypropylene upon exposure to accelerated weathering

Nora Meides<sup>1†</sup>, Anika Mauel<sup>2†</sup>, Teresa Menzel<sup>3</sup>, Volker Altstädt<sup>3</sup>, Holger Ruckdäschel<sup>3</sup>, Jürgen Senker<sup>2</sup> and Peter Strohriegl<sup>1\*</sup>

## Abstract

Polymers are omnipresent in our everyday lives. For specific applications, their properties can be extensively modified by various types of additives, e.g., processing stabilizers, antioxidants, UV-stabilizers, flame retardants, and plasticizers. While several additives are nowadays considered to be toxic or persistent in the environment, quantitative data characterizing plastic fragmentation and microplastic formation have not yet been discussed in detail. Here, we present a long-term, laboratory-controlled accelerated weathering study on polypropylene (PP) particles with and without processing stabilizers. We were able to identify the stabilizers as Irgafos<sup>®</sup> 168, and Irganox<sup>®</sup> 1010. For both PP sample sets, we monitored the degradation using a combination of various analytical methods, such as gel permeation chromatography, particle size distributions, scanning electron microscopy, solid-state <sup>13</sup>C magic-angle spinning NMR and liquid-state <sup>1</sup>H, <sup>13</sup>C, <sup>31</sup>P NMR spectroscopy, differential scanning calorimetry and matrix-assisted laser desorption ionization time of flight mass spectrometry. The stabilizers prevent degradation by simulated solar radiation for about 350 h. Then, degradation sets in rapidly, leading to an exponential decrease in molecular weight and particle size, accompanied by an increase in crystallinity and the formation of oxygen-containing functional groups. After 3200 h, representing approximately 2 years of outdoor weathering, both PP samples exhibit comparable characteristics and sizes, regardless if a stabilizer was initially present. During degradation, an extremely large number of 100,000 daughter particles (4 μm) are formed and released from one MP particle of 192 μm diameter. Their physical properties and chemical composition have largely changed, resulting in a very low molecular weight and a hydrophilic character. These particles no longer resemble pristine PP. We thus expect them to be more prone to biodegradation compared to the starting material.

**Keywords:** Degradation, Microplastic, Nanoplastic particles, Photooxidation, Additives, Secondary daughter MP particle production

## Introduction

Plastics are nowadays inevitably a part of our everyday life. They are cheap, lightweight, and durable, and their properties can be easily adapted, leading to a wide range of applications. In 2019, the global plastic production reached a total of 368 million tons, still increasing year by year [1]. The largest end-use market in Europe, with a contribution of 40%, is the packaging industry, where polypropylene (PP) is one of the dominating polymer types [1]. Materials made of PP are often single-use items

<sup>†</sup>Nora Meides and Anika Mauel contributed equally to this work and share first authorship.

\*Correspondence: peter.strohriegl@uni-bayreuth.de

<sup>1</sup> Department of Macromolecular Chemistry I, University of Bayreuth, Universitätsstraße 30, 95447 Bayreuth, Germany  
Full list of author information is available at the end of the article

for wrappers, food packaging, containers and bottle caps. This leads to the generation of large amounts of PP waste, often exported to developing countries with poor waste management strategies [2, 3]. Ultimately, a large amount of the exported waste is expected to end up in environmental compartments, where abiotic and biotic degradation mechanisms lead to fragmentation and break-down [2, 4, 5]. As a consequence, microplastic (MP) is formed, often defined as plastic fragments of all polymer types and shapes with the largest dimension ranging from 1  $\mu\text{m}$  to 1000  $\mu\text{m}$  [6]. In recent years, MP has become a great concern and is seen as an emerging ecological risk [7–10].

Not only are large quantities of secondary MP formed from degradation and fragmentation, their chemical structure is also modified throughout the ageing process. The initially non-polar polymer chains turn gradually into increasingly polar oligomers [5, 11, 12]. As a consequence of pronounced oxidation, aged MP particles become hydrophilic, enhancing biofilm formation [13, 14] as well as the uptake by organisms [15, 16]. Recent studies have addressed the toxicity of small polymer MP particles [17] and negative effects on organisms [18, 19].

Toxicity may not only originate from the polymer itself or from changes in the chemical composition during weathering but can also result from leaching and degradation of low molar mass compounds present in almost all polymers. Plastics for everyday products are optimized to maintain their properties for a specific period of time. For this purpose, a variety of additives are used to stabilize the polymers a) during processing and b) during their service life. With regard to their application, different classes of additives are distinguished such as processing aids, antioxidants, thermo- and UV-stabilizers, flame retardants and plasticizers [20]. Some low molar mass compounds frequently present in consumer products and plastic packaging, are now considered environmentally harmful or even toxic, such as phthalates, bisphenol A, biocides, certain flame retardants, and highly fluorinated substances [21]. Consumer goods and packaging products are very complex materials containing a variety of substances [22]. This complexity is maintained or even increases once polymer materials of any origin are released into natural compartments. The incorporated stabilizers and their degradation products can leach from the plastics, posing an environmental concern [20].

In recent years, multiple studies have addressed the environmental weathering of PP, polystyrene (PS), and polyethylene (PE), reporting changes in chemical composition, a decrease in molecular weight due to chain-scission and the formation of degradation products such as peroxides, alcohols, and carboxylic acids [23–29]. These changes are induced by photooxidation and

typically accompanied by a modification of the physical properties, leading to embrittlement and fragmentation [5, 7, 30–32]. In natural compartments, physical stress factors such as mechanical impacts will additionally enhance fragmentation and break-down, leading to MP formation [33].

Photooxidation of polymers and the influence of polymer additives on polymer break-down has been thoroughly investigated for the past decades [34–36]. While the underlying mechanisms of photooxidative degradation are well understood, much less is known about the role of stabilizers and their degradation products [20]. Quantitative data regarding fragmentation rates as well as secondary MP particle production and release remain scarce [32, 37–40], and are lacking for stabilized polymer systems. Furthermore, numeric data for time scales in which the stabilizers avoid degradation, and the effect of the stabilizers on the fragmentation of macroplastic has only gained little attention up to date.

To bridge this knowledge gap, we combined laboratory weathering with extensive analytical investigations and calculation of fragmentation rates for a commercially available stabilized PP. In order to monitor the influence of stabilizers on the polymer degradation, with special focus on the fragmentation into smaller particles, the stabilizers were removed from a second PP batch by Soxhlet extraction and identified. A multitude of analytical methods, such as gel permeation chromatography (GPC), light scattering for particle size distributions, scanning electron microscopy (SEM), and differential scanning calorimetry (DSC) were combined to trace the degradation and fragmentation of stabilized, and non-stabilized PP as a function of exposure time.

Additionally, solid-state  $^{13}\text{C}$  magic-angle spinning (MAS) NMR spectroscopy was performed for identification and quantification of photooxidative defects accumulating with proceeding degradation. As previously reported [5, 41] quantification is enabled by a multiple cross polarization (multiCP) pulse sequence [42, 43]. Although solid-state NMR spectroscopy has rarely been considered for investigation of degradation products, it serves as a complementary method to other commonly used techniques, such as Fourier transform infrared (FTIR) or Raman spectroscopy, and pyrolysis–gas chromatography–mass spectrometry (Py-GC–MS) [23, 24, 28, 29, 44–46]. NMR spectroscopy provides volume-averaged results and can give information on the dynamics of the system, e.g., details on the distribution and variations of crystalline and amorphous regions. It is a non-destructive method however, it does require relatively large amounts of sample material, which can pose a problem for environmental samples.

The data presented in this study deliver a profound understanding of fragmentation rates resulting from photooxidative degradation, also considering the influence of stabilizers. The derived numbers give an approximation for how many micro- and nanoplastic particles can potentially be released, when PP is exposed to solar radiation and mechanical stress in an aqueous environmental setting. Experimentally determined numerical fragmentation rates have not yet been reported in the literature. Thus, this study fills a knowledge gap and delivers important information concerning micro- and nanoplastic formation.

## Experimental

### Material and methods

Polypropylene (PP, Moplen HP526J) in pellet form was provided by LyondellBasell Industries (Basell Polyolefine GmbH, Wesseling, Germany). As stated in the data sheet, this PP grade is supplemented with a standard processing stabilizer. Particles were produced from PP pellets by cryo-milling with an ultra centrifugal Mill ZM-200 (Retsch GmbH, Haan, Germany). Particles were then separated into several fractions using an Alpine air jet sieve E200 LS (Hosokawa Alpine AG, Augsburg, Germany). For the experiments from this study, the fractions < 125  $\mu\text{m}$  and 125–200  $\mu\text{m}$  were used. Reference compounds Irgafos<sup>®</sup> 168 (Tris(2,4-di-tert-butylphenyl)phosphate), and Irganox<sup>®</sup> 1010 (Pentaerythritol tetrakis(3-(3,5-di-tert-butyl-4-hydroxyphenyl)propionate)) were purchased from BASF (Ludwigshafen, Germany). 500 mg Irganox<sup>®</sup> 1010 was dissolved in 100 ml tetrahydrofuran (THF) and placed into the Q-Sun Xe-3 for 100 h. THF was then evaporated to dryness and the compound, further referred to as Irganox<sup>®</sup> 1010<sub>weathered</sub>, was analyzed via MALDI-TOF MS.

### Soxhlet extraction

A Soxhlet extraction was performed on a PP fraction < 125  $\mu\text{m}$  in size. 24 g PP particles were placed into a glass thimble onto a cellulose filter and covered with glass wool. Extraction was performed in a Soxhlet apparatus with 700 ml of boiling THF for 14 days. Particles were filtered off and dried under vacuum (40 °C) and subsequently weathered according to the procedure described below. The extraction solvent was evaporated, and the residue was dissolved in hexane and ethyl acetate (19:1) and passed over a silica column. The products were investigated via MALDI-TOF MS.

### Matrix assisted laser desorption ionization-time of flight mass spectrometry (MALDI-TOF MS)

The residue of the stabilizer extraction, as well as Irganox<sup>®</sup> 1010<sub>weathered</sub>, were analyzed via MALDI-TOF

MS using the solvent-based dried droplet sample preparation procedure. Sample and matrix (DHB – 2,5-dihydroxybenzoic acid) were dissolved in THF with a concentration of 10 mg/ml, mixed with a ratio of 5:20 and a thin layer applied onto the target plate. Mass spectra were acquired with a Bruker autoflex<sup>®</sup> maX TOF/TOF (Bruker Daltonics GmbH & Co. KG, Bremen, Germany) in positive ion reflector mode between 200–2000 Da. The instrumental settings were optimized for best resolution and highest intensity. In total, 5000 shots were taken randomly across the dried-droplet sample spot. The obtained spectra were processed with the flexAnalysis software.

### Accelerated weathering

Both stabilized and unstabilized particle fractions were weighed to 20 g each and transferred into quartz glass beakers filled with 600 ml deionized water and covered with quartz glass lids. Stirring of the water-particle mixture was enabled using magnetic stirrers and PTFE-covered stirring devices. This setup was placed into a Q-SUN XE-3 test chamber (Q-LAB Corporation, Westlake, OH, USA) and irradiated for a total of 3200 h. The test chamber is equipped with three xenon lamps, operating at 60 W/m<sup>2</sup> each (at 300–400 nm), which corresponds to a total irradiance of 594 W/m<sup>2</sup> (300–800 nm) and a five-fold acceleration compared to mid-European conditions (Fig. S1, Tab. S1). This acceleration resembles approximately two years of outdoor weathering in central Europe. Further, Daylight-Q filter systems, cutting off radiation with wavelengths < 295 nm, were installed. This assures an irradiation spectrum very similar to the spectrum of natural sunlight (Fig. S2). Additional settings were relative humidity at 50% and chamber temperature at 38 °C.

At each sampling time (24, 50, 100, 200, 400, 600, 800, 1200, 1600, 2000, 2400, 2800 and 3200 h), 1–2 g of sample material were drawn from the water-sample mixture, filtered, and dried under vacuum at 40 °C. Samples were stored in a dark and dry place until further analysis.

### High temperature gel permeation chromatography (HT-GPC)

Molecular weight distributions (MWD) as well as  $M_n$ ,  $M_w$ , and  $\bar{D}$  values were measured via GPC using an Agilent (Polymer Laboratories Ltd.) PL-GPC 220 high-temperature chromatographic unit. This set is equipped with RI and PD detectors as well as three linear mixed bed and guard columns (Olexis). Analysis was performed at 150 °C (Pasch, 2001) using 1,2,4-trichlorobenzene (TCB) as the mobile phase. All samples were prepared by dissolving 2–3 mg of PP particles (0.1 wt.-%) in 1.5 ml of the mobile phase solvent (TBC) in an external oven at 150 °C

upon continuously stirring. The solutions were run without filtration. The determined molecular weights were referenced to linear HDPE standards ( $M_w = 142,000 - 701,000$  g/mol,  $K = 40,600$ , and  $\text{Alpha} = 0.725$ ) and were corrected with  $K$  and  $\text{Alpha}$  values for *i*-PP ( $K = 19,000$  and  $\text{Alpha} = 0.725$ ).

### Scanning electron microscopy (SEM)

Field-emission scanning electron microscopy (FESEM) was performed on particles with a Zeiss ULTRA PLUS (Carl Zeiss Microscopy GmbH, Jena, Germany) at an acceleration voltage of 3 kV and a FEI Quanta 250 (Field Electron and Ion Company, Thermo Fisher Scientific, Hillsboro, USA) high resolution field emission gun (FEG) scanning electron microscope at 10 kV, operating at low vacuum. Particles were coated with a thin layer of platinum by a Cressington 208 HR sputter coater prior to investigation.

### Particle size analysis

Particle size distributions and the average particle size were determined with a Microtrac FlowSync Particle Size Analyzer (Microtrac Retsch GmbH, Haan, Germany) having a lower detection limit of 10 nm. Measurements were performed in deionized water with 2–5 mg of particles. 2 ml of 5 wt.-%  $\text{Na}_4\text{P}_2\text{O}_7$ , and a few drops of a 2 wt.-%  $\text{C}_{20}\text{H}_{37}\text{NaO}_7\text{S}$  (dioctyl sulfosuccinate sodium salt) detergent were added and 60 s of ultrasound at 40 kHz were applied to avoid aggregation. Average values from three measurements were calculated by the Microtrac software.

### Differential scanning calorimetry (DSC)

DSC measurements were performed on 8–10 mg sample material using a Mettler Toledo DSC 3+ (Mettler-Toledo GmbH, Gießen, Germany). The samples were heated with 10 K per minute under  $\text{N}_2$ -atmosphere from 25–200 °C and cooled to 25 °C. An isothermal stage of 5 min was applied between the heating and the cooling cycle. The degree of crystallinity  $\chi_c$  in the first heating cycle was determined using  $\Delta H_m^0 = 207.1$  J/g for a hypothetically 100% crystalline PP [29]. Determination of  $\chi_c$  and  $T_m$  was performed using the STARe software.

### NMR spectroscopy

Liquid-state  $^1\text{H}$ ,  $^{13}\text{C}$  and  $^{31}\text{P}$  NMR spectroscopic experiments were recorded on a Bruker Avance-III HD spectrometer with 5 mm CryoProbe™ Prodigy BBO 500 S2 head operating at a  $B_0$  field of 11.7 T ( $^1\text{H}$ :  $\nu_0 = 500.1$  MHz,  $^{13}\text{C}$ :  $\nu_0 = 125.8$  MHz,  $^{31}\text{P}$ :  $\nu_0 = 242.9$  MHz). Deuterated chloroform ( $\text{CDCl}_3$ ) was used as solvent. Via the residual solvent resonance all  $^1\text{H}$  and  $^{13}\text{C}$  spectra were referenced to tetramethylsilane. For the  $^{31}\text{P}$

spectra, triphenylphosphine oxide was used as secondary standard.

Solid-state  $^{13}\text{C}$  MAS NMR spectroscopic experiments were recorded on a Bruker Avance-III HD spectrometer operating at a  $B_0$  field of 9.4 T ( $^1\text{H}$ :  $\nu_0 = 400.1$  MHz,  $^{13}\text{C}$ :  $\nu_0 = 100.6$  MHz) using a 3.2 mm triple resonance probe (Bruker) with zirconia rotors (approx. 25 mg sample). A spinning frequency of 20 kHz was applied which is sufficiently fast to avoid the occurrence of spinning sidebands as the chemical shift anisotropies (20–40 ppm) of aliphatic carbons are averaged [47].  $^{13}\text{C}$  CP experiments were performed for a series of PP samples with different weathering times. The contact time was set to 2.0 ms, and the same Hartmann-Hahn conditions as for the multiCP experiments were used. MultiCP measurements [43] were conducted for the longest weathered sample. The parameters for the multi-pulse CP measurements [42] were optimized for the PP samples. Seven CP blocks with a contact time of 400  $\mu\text{s}$  ( $\nu_{\text{mut}}(^{13}\text{C}) = 47$  kHz,  $39 \text{ kHz} \leq \nu_{\text{mut}}(^1\text{H}) \leq 55 \text{ kHz}$ ), separated by a time  $t_z$  of 3 s, were applied. At the end and the beginning of each CP block ( $90^\circ_x$ ) pulses with pulse lengths of 2.5  $\mu\text{s}$  ( $^1\text{H}$ ) and 3.8  $\mu\text{s}$  ( $^{13}\text{C}$ ) were used. Proton decoupling was applied during acquisition using the spinal-64 sequence at a  $B_1$  field of 70 kHz.

For defect quantification, all spectra were deconvoluted with pseudo-Voigt profiles using the SOLA program included in TopSpin 3.2 (Bruker). To account for the small defect proportions, a serial refinement procedure was applied. For the two spectra with longest weathering times and thus highest defect proportions, simultaneous, free refinements with one set of isotropic chemical shift, line broadening and Gauss/Lorentz ratio, for each defect resonance, were performed. The corresponding intensities were refined separately. For shorter weathering times, the obtained fitting parameters were applied in subsequent refinements, and only the intensity was varied. This reduces the degrees of freedom sufficiently, allowing to derive meaningful intensities for spectra with lower signal-to-noise ratios. In contrast, for the more intense backbone signals, a free refinement of all parameters was possible. All refinement parameters are given in Table S5.

## Results and discussion

We performed accelerated weathering laboratory experiments under abiotic conditions, using particles of a standard PP grade. To elucidate the influence of stabilizers on the degradation, we used one batch with and one batch without stabilizers.

Using MALDI-TOF MS and  $^1\text{H}$ ,  $^{13}\text{C}$  and  $^{31}\text{P}$  liquid-state NMR spectroscopy, the Soxhlet extracted additives were analyzed and two stabilizers could be identified.

The MS spectra are shown in Figures S3A and S4A + B. Three peaks at  $m/z$  663.2,  $m/z$  685.2 and  $m/z$  701.2 are dominant in Figure S3A. They match values for tris(2,4-di-tert-butylphenyl)phosphate, the oxidized species of the well-known stabilizer Irgafos<sup>®</sup> 168 [48, 49]. Tris(2,4-di-tert-butylphenyl)phosphite (Irgafos<sup>®</sup> 168) itself could not be detected. These findings were validated by the obtained NMR spectra (Fig. S5A-C) exhibiting the typical resonances for tris(2,4-di-tert-butylphenyl)phosphate. In particular, the <sup>31</sup>P NMR spectrum (Fig. S5C) shows a single resonance at -19.9 ppm, demonstrating, that only the phosphate is present. Additionally, Irganox<sup>®</sup> 1010 could be identified as a second stabilizer by analysis of Irganox<sup>®</sup> 1010 reference material, treated with simulated solar radiation in THF for 100 h (Irganox<sup>®</sup> 1010<sub>weathered</sub>). The dominant peaks observed in the MALDI spectra of the extracted stabilizer (Fig. S4A) and in Irganox<sup>®</sup> 1010<sub>weathered</sub> (Fig. S4B) are almost identical and represent fragments of the original Irganox<sup>®</sup> 1010 molecule (Fig. S4C). These observations could be confirmed by <sup>1</sup>H and <sup>13</sup>C liquid-state NMR spectra (Fig. S5D-E).

Since Irgafos<sup>®</sup> 168 and Irganox<sup>®</sup> 1010 are processing stabilizers, their main purpose is to assure stability of the respective polymer during melt processing, e.g. extrusion [48]. Temperature, shear strain, or other critical factors may lead to chemical degradation, reducing the molecular weight, and resulting in a decrease of the mechanical strength. To assure stability throughout melt processing, stabilizers, such as radical scavengers and hydroperoxide decomposers, are often added. Irgafos<sup>®</sup> 168 is a hydrolytically stable phosphite processing stabilizer acting as a secondary antioxidant [50]. It is often used in combination with the primary antioxidant Irganox<sup>®</sup> 1010, a sterically hindered phenol. By deactivation of peroxy radicals and hydroperoxides, formed during autoxidation, degradation of the polymer is prevented. The most important

reactions during the decomposition of PP are shown in Figure S6 [49, 51]. The mechanism is very similar for both, thermal and photochemical decomposition. The major difference is, that the energy to create free radicals by a homolytic cleavage of C-H bonds comes from heating, in the case of thermal oxidation, and from high energy photons of the sunlight, in the case of photooxidation. In natural environments, photooxidation is the dominating mechanism to induce degradation. Following the initial formation of radicals, a multitude of reactions proceed via hydroperoxides, and peroxide and alkoxy radicals, leading to chain-scission and crosslinking (Fig. S6, top scheme). The chain-scissions are accompanied by the formation of oxygen-containing functional groups like alcohols, ketones and carboxylic acids. The stabilizer combination is able to prevent decomposition by reacting with all reactive intermediates marked in red in Figure S6 (top scheme). Thereby, the stabilizer combination, which is usually added in quantities of ~0.1 to 0.2 wt.% [51], retards degradation up to the point where it is completely consumed. Afterwards, degradation sets in.

To study the degradation of PP, particles were irradiated with simulated solar radiation, while being stirred in water and thus subjected to additional mechanical stress. Degradation of both sample sets, with a special view on the influence of the stabilizers, was monitored over a total experimental duration resembling approximately two years of outdoor weathering under mid-European conditions.

#### Particle size

Values for the average particle size are displayed in Figure 1 (Tab. S2) and particle size distributions in Figure S7. To ensure efficient extraction of the additives, a smaller particle fraction was chosen for unstabilized PP ( $\varnothing = 119 \mu\text{m}$ ) compared to the stabilized particle

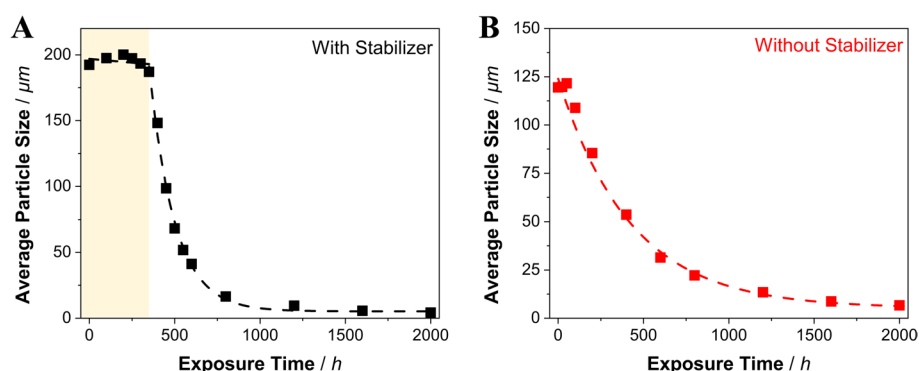


**Fig. 1** Average particle size for **A** PP particles with stabilizer and **B** PP particles without stabilizer. The induction phase, characterized by the presence of Irgafos<sup>®</sup> 168 and Irganox<sup>®</sup> 1010, is highlighted in yellow. Degradation proceeds in an exponential manner with  $\tau = 149$  h for PP with and  $\tau = 427$  h for PP without stabilizer ( $\propto \exp(-t/\tau)$ )

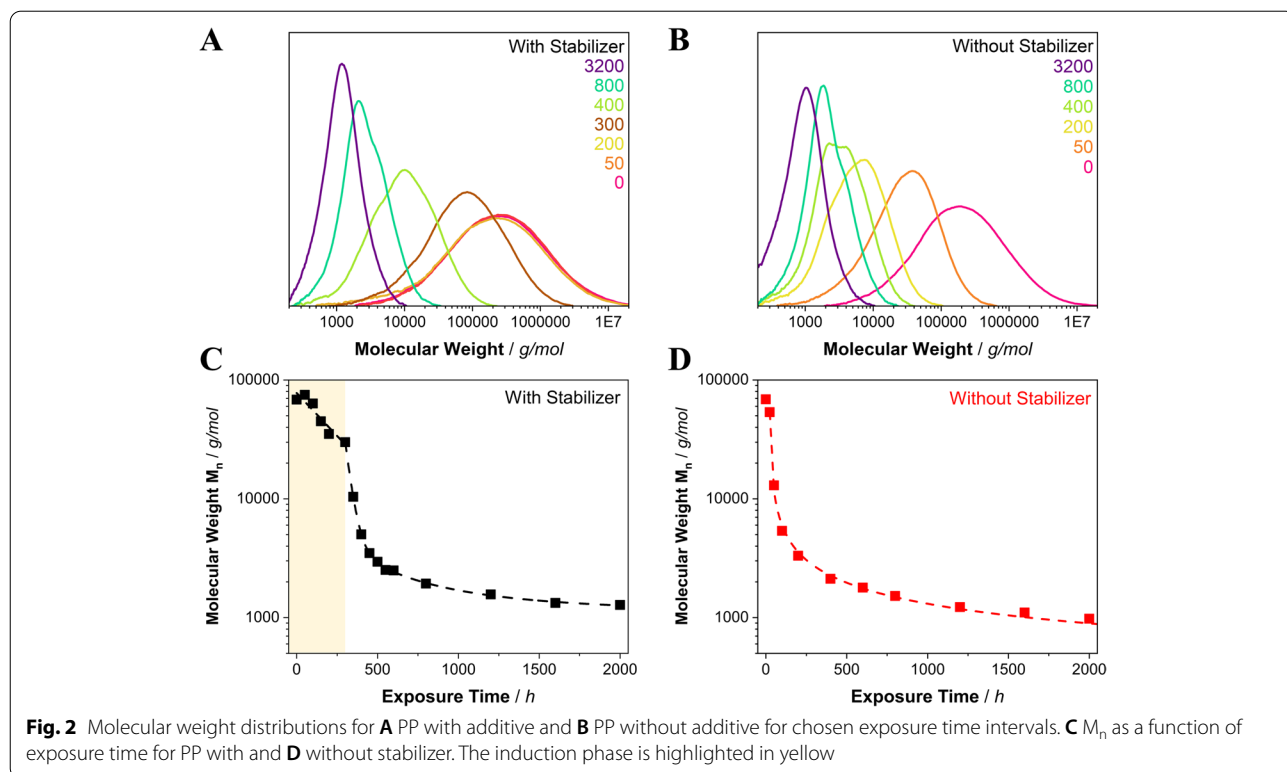
fraction ( $\phi = 192 \mu\text{m}$ ). The average size of the particles with stabilizer in Figure 1A remains constant up to 350 h, then rapidly decreases in an exponential manner. We attribute the linear trend between 0–350 h to the influence of the stabilizer, since it is absent for PP without additives (Fig. 1B). We refer to this phase as the induction phase, highlighted in yellow in Fig. 1. The exponential fit from 350 h onwards, reveals a lifetime  $\tau$  of 149 h, in which the particles have reached half of the original size. PP particles without stabilizer (B) start to decrease already from 50 h onwards, but decay slower, with  $\tau = 427$  h. After 800 h, both samples reach the same particle size of  $\sim 20 \mu\text{m}$ , which slowly decreases further to  $\sim 5 \mu\text{m}$  in the remaining 2400 h of experiment duration (Tab. S2). During weathering the particle size distribution broadens, as can be seen in Figure S7. Further details on the particle size at long irradiation times will be discussed in the upcoming sections.

#### Molecular weight distributions

Molecular weight distributions (MWD) for both sample sets were obtained by HT GPC (Tab. S3, Fig. S8). Initially, MWDs from both experiments are broad (Fig. 2A, 2B) with dispersity ( $\mathcal{D}$ ) values of  $>7$ , typical for commercial PP. Throughout the exposure to simulated solar radiation, PP particles are highly affected by photooxidation, radical formation and chain scission. The  $M_n$  decreases

from  $M_{n,0} = 68,000 \text{ g/mol}$  down to  $M_{n,3200} \sim 1000 \text{ g/mol}$  within 3200 h (Tab. S3). Major differences between the stabilized and non-stabilized PP are evident within the first 300 h of weathering. The PP sample with stabilizer shows a uniform MWD (Fig. 2A) with curves from 0–250 h overlapping. The  $M_n$ -values (Fig. 2C) decrease very slowly in a linear trend until 300 h, then evolve in an exponential manner, revealing rapid decrease of the polymer chain length. This linear trend represents the induction phase, which was also observed within the particle size data (Fig. 1). The PP sample without stabilizer shows an immediate shift of the MWD to lower values and a reduction of  $M_n$ , starting with the first sample drawn after 24 h (Fig. 2B, 2D, S8).

Within both, the particle size measurements (Fig. 1A) and the MWD (Fig. 2A), PP with stabilizer shows only little effects from weathering with steady values in particle size and only slow decrease in molecular weight  $M_n$  in the beginning. This is due to the deactivation of reactive intermediates from autoxidation by Irgafos<sup>®</sup> 168 and Irganox<sup>®</sup> 1010. Once degradation starts, it proceeds rapidly and in an exponential manner, catching up with the non-stabilized PP within few sampling times.  $M_n$  values are similar ( $\sim 2000 \text{ g/mol}$ ) for both PP samples after 800 h of weathering (Tab. S3). Fragmentation however proceeds far faster for the stabilized PP from 350 h onwards, than what is observed for the non-stabilized PP, which

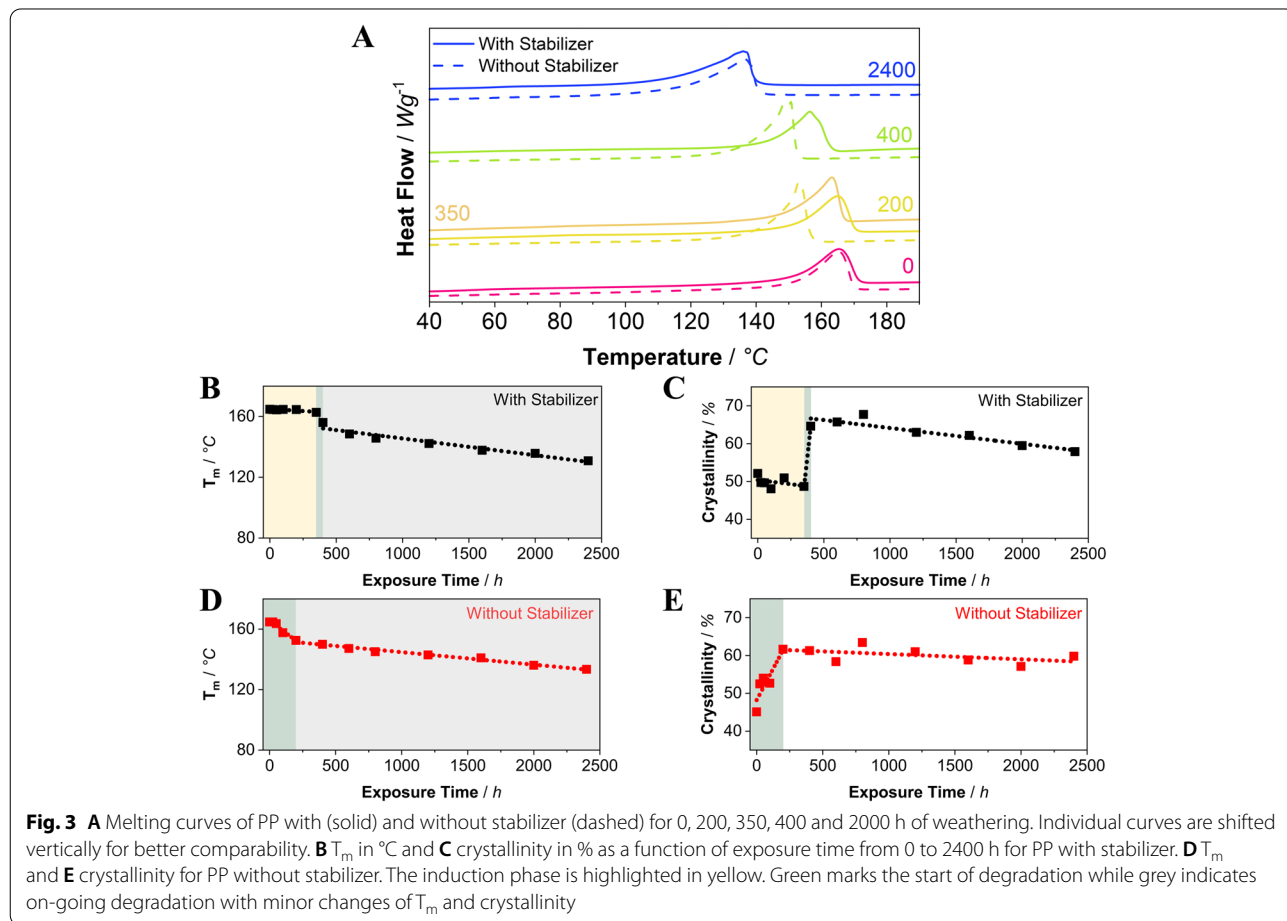


degrades from 50 h on. This is a striking observation. The only difference between the two PP samples is the presence of stabilizers and predominantly their degradation products in the stabilized PP sample, in the time interval where particle size decreases in an exponential manner. Both, stabilizers and degradation products are absent in the non-stabilized PP sample. We speculate that the presence of the degradation products may be responsible for the faster fragmentation, and thus the lower value of  $\tau$  determined for the exponential decay of the stabilized sample. After 3200 h, the average particle size, as well as the final MW, are almost equivalent for samples with and without stabilizer.

**Crystallinity and melting temperature**

The thermal characteristics of PP with and without stabilizer were investigated via DSC and are shown in Fig. 3 (Fig. S9). The melting temperature  $T_m$  and degree of crystallinity  $\chi_c$  for the reference sample were determined to  $T_{m,0} = 165\text{ }^\circ\text{C}$ ;  $\chi_{c,0} = \sim 50\%$  (Tab. S4). Heating curves for both PP experiment series, displayed in Fig. 3A, show similarities for PP with stabilizer (solid lines) at 0 and

200 h, while PP without stabilizer (dashed lines) shifts to lower values. The influence of the stabilizer within the first 350 h becomes evident when looking at  $T_m$  (Fig. 3B, 3D) and trends for the degree of crystallinity  $\chi_c$  (Fig. 3C, 3E) for both PP experiments. No change in  $T_m$  can be detected within the induction phase of stabilized PP, highlighted in yellow (Fig. 3B, 3C). The start of degradation is marked in green, with a prominent drop in  $T_m$  by  $\sim 6\text{ }^\circ\text{C}$ . The decrease in  $T_m$  can be explained by increasing crystal defects occurring as a consequence of degradation [29]. As degradation continues (grey),  $T_m$  decreases further from  $156\text{ }^\circ\text{C}$  to  $120\text{ }^\circ\text{C}$  (Tab. S4). This is accompanied by a broadening of the melting peak (Fig. 3A), and an increase in the melting enthalpy  $\Delta H_m$ . From integration of the melting peak,  $\chi_c$  was determined, and a similar trend is observed (Fig. 3C): no change in  $\chi_c$  within the induction phase, followed by a rapid increase by 17%, marking the beginning of degradation. For PP without stabilizer, the induction phase is absent, and degradation is initiated directly.  $T_m$  decreases by  $13\text{ }^\circ\text{C}$  with a linear trend from 0–200 h and  $\chi_c$  increases by 17%. The long-term degradation proceeds similar for both PP experiments.



The  $^{13}\text{C}$  CP MAS NMR spectra for both sets of weathering experiments (with and without stabilizer combination) show the typical resonances for the amorphous and crystalline regions of PP [52] (Fig. S10, S11). The intensity of the crystalline region increases fast up to 200 h. For longer weathering times, the lineshape does not change significantly anymore. For stabilized PP, a similar trend is observed, which is delayed by roughly 200 h, marking the induction period where the stabilizers are consumed. These trends are in line with the conclusions drawn from the DSC measurements. For longer weathering times, the spectral overlap is, however, too strong to allow for quantitative analysis of the spectral intensities, and thus for calculation of the degree of crystallinity.

The thermal and NMR characteristics for both PP experiments correlate well with the observation previously made for MW and MWD (Fig. 2). For semi-crystalline polymers, chain-scission takes place mainly in the amorphous regions. The disassembled polymer chains then rearrange due to the high mobility of the chains within the temperature range of our experiments, which is well above the glass-transition temperature of PP. The

chains rearrange in a preferably ordered way, which leads to an increase in crystallinity [53]. These chain dynamics also influence the particle fragmentation and hinder crack-formation. In early weathering stages (0–350 h, Fig. 1A) the particle size thus remains constant, while molecular weight values already indicate a slow decrease in chain length from chain-scission (Fig. 2C). At late stages of degradation, the crystallinity for both PP samples slowly decreases again (Fig. 3C, 3E). We explain this saturation effect by an increasing amount of polar polymer defects [29] hindering the alignment of the residual short polymer chains. Our observations match previous studies, investigating the environmental degradation of PP, where an increase in crystallinity is reported [54, 55] along with a decrease in the MW [55].

#### Development of chemical functional groups

To trace the continuous degradation by quantifying chain-scissions and formation of chemical functional groups,  $^{13}\text{C}$  CP MAS NMR spectra were recorded for both sets of weathering experiments (Fig. 4A, 4B). Compared to the reference material, additional peaks develop,

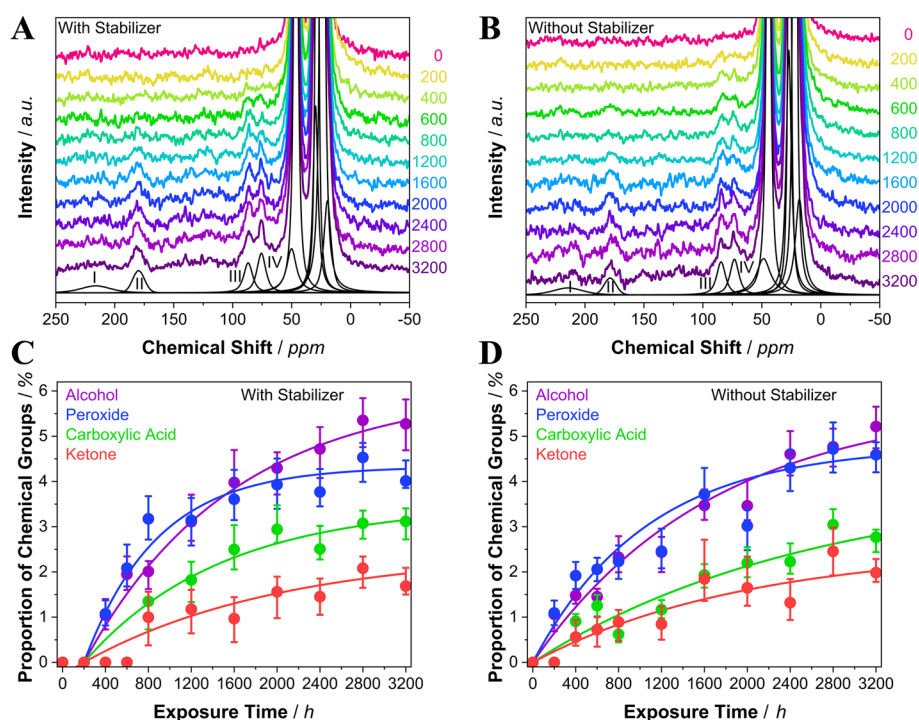


**Fig. 4.**  $^{13}\text{C}$  CP MAS NMR spectra of **A** PP with stabilizer and **B** without stabilizer for different weathering times. Upon irradiation, the generation of new signals assigned as signals I (ketone), II (carboxylic acid), III (peroxide) and IV (alcohol) is observed [56, 57]. No refinement of vinylidenes was performed between 100–150 ppm, since the resonances of the decomposition products of Irgafos<sup>®</sup> 168 superimpose with the vinylidene resonances. The spectra are normalized to the intensity of the methyl sidechain carbon signal (at approx. 24 ppm). Individual spectra are shifted vertically for better comparability. Exemplarily, the individual fits for the peaks in the spectrum of the 3200 h weathered particles are shown as black lines; Derived proportions (SI Eq. 2 - Eq. 6) of alcohols, peroxides, carboxylic acids and ketones, as functions of the exposure time, for PP particles **C** with and **D** without stabilizer. Trend curves with exponential build-up and an induction period (PP with stabilizer) are included as guide for the eye

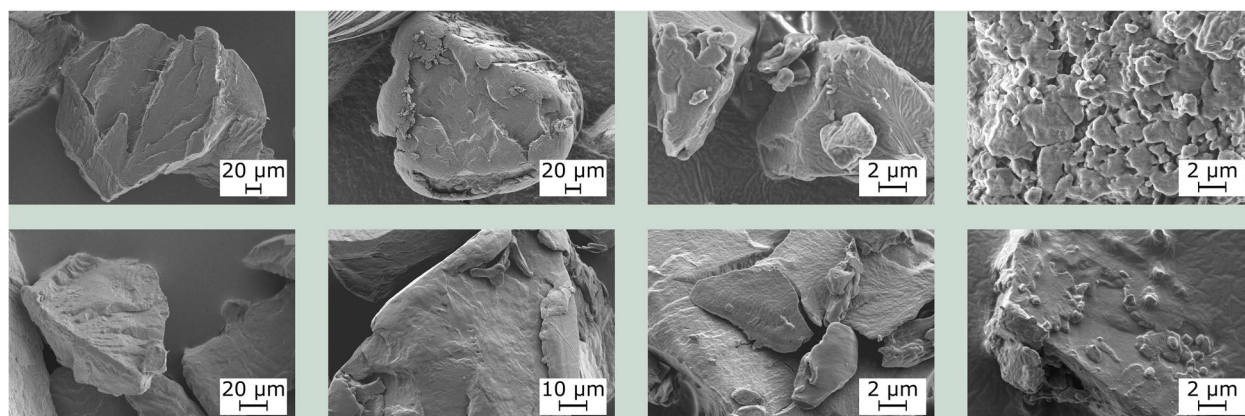


**Fig. 5** A-D SEM images of PP with stabilizer and E-H without stabilizer. A&E Virgin particles, reference material, B&F smoothed particles after 200 h, C&G particle fragments after 800 h and D&H particle surfaces after 2000 h. Smaller particles in the nanometer-range are visible on the surfaces

gaining intensity with increasing exposure time. These peaks could be assigned to the degradation products of PP depicted in Figure S6, as ketones (215 ppm), carboxylic acids (179 ppm), peroxides (85 ppm) and alcohols (74 ppm) [56, 57]. Due to the low intensity in the spectral range typical for ketones, end-chain and in-chain ketones [56] are handled as one broad resonance (Fig. S12). Further details on the refinement procedure are given in the section “Experimental”. Quantification was achieved by calibrating the CP spectra to a quantitative multi CP experiment, as previously described [43]. The proportions of the chemical groups are displayed in Fig. 4C and 4D. The defect resonances of the stabilized PP (Fig. 4C) remain below the detection limit during the first 200 h of exposure, which is in accordance with the presence of the induction phase. Between 200 and 800 h, a rapid increase for the proportions of all defects occurs. For longer exposure times, a turnover to an attenuated increase was observed. In the case of non-stabilized PP (Fig. 4D), photooxidation sets in with the start of the weathering experiments. Nevertheless, also for this sample a turnover to a smaller photooxidation rate was found with an onset of 400 h exposure time. In both cases, the highest proportions of the polar defects were observed for peroxide and alcohol groups, followed by carboxylic acids. Ketone defects play only a minor role and were observable only for larger weathering times. We attribute the high peroxide and alcohol proportions to the large number of tertiary C-atoms, forming stable radicals and subsequently peroxides and alcohols [27].

#### Particle surface and degradation characteristics

The changes in particle size and shape during the degradation of PP have been visualized by SEM. A selection of images from experiments with and without stabilizers

are displayed in Fig. 5. More images are given in Figures S13 and S14. Aside from the difference in particle size between both fractions, surface characteristics for both particle fractions are very similar (Fig. 5, S13, and S14). The reference sample before irradiation consists of particles with rough shapes and harsh edges, resulting from cryo-grinding (Fig. 5A, 5E). Within the first stage of weathering, particle edges start to smoothen and are rounded off (Fig. 5B, 5F). With continuous exposure to simulated solar radiation and mechanical stress, particles start to disintegrate to average particle sizes < 10 μm for both experiments (Tab. S2). Dominant crack patterns are absent upon break-down, which can be attributed to the high flexibility of PP at ambient temperature, resulting in self-healing by surface rearrangement of the polymer chains [58]. This is in accordance with the interpretation of the thermal characteristics determined from DSC (Fig. 3C, 3E) and NMR spectroscopy (Fig. S11).

Recently, we developed a three-stage degradation model for semi-crystalline, non-stabilized polymers, using unstabilized LDPE as exemplary material [41]. Stage I represents surface abrasion, characterized by a roughly constant particle size, accompanied by a rounding of the particle surface. In stage II fragmentation starts, particle size decreases, the molecular weight is reduced and first chemical functional groups can be identified. The final stage III represents the formation of a large number of small microplastic and nanoplastic (NP) particles. They likely agglomerate, as a result of their high surface-to-volume ratios and an increasingly polar surface, resulting from the large number of oxygen-containing functional groups.

Our three-stage model is also applicable to PP without stabilizer. However, the transition from stage I to stage II is very short, which is evident in the particle size and

MW measurements (Fig. 1B, Fig. 2D). This behavior is related to the chemical structure of PP. Every second carbon in the PP backbone is a tertiary C-atom, making PP very susceptible to photooxidation. The single H-atoms of tertiary C-atoms are prone to abstraction, leading to the formation of a large number of stable radicals [27], which is also evident in the proportion of chemical groups developing (high proportion of peroxides and alcohols, Fig. 4C, 4D). Once degradation is initiated, it proceeds in an autocatalytic manner [59]. Consequently, solar radiation leads to a rapid polymer break-down in the absence of a stabilizer.

Fragmentation sets in together with a loss of MW (stage II), leading to embrittlement. This results in particle break-up and the formation of large quantities of secondary daughter MP particles and a rapid decrease in particle size (Fig. 1B). Due to surface-healing by rearrangement of the polymer chains above  $T_g$  [58], no microcracks could be observed. With further weathering, decreasing particle size and accumulation of degradation products, the particle properties change. Stage III is initiated with the average particle size having decreased 10 times. A multitude of daughter particles are formed from disintegration, reaching sizes  $< 10 \mu\text{m}$ , and even ranging down to the nanometer scale (Fig. 5D, 5H). They contain a high content of oxidation products and are highly polar. Due to their large surface-to-volume-ratio and polarity, MP and NP particles have a strong tendency to agglomerate (Fig. 5D, 5H) and almost no free NP particles with sizes  $< 1 \mu\text{m}$  could be observed in our particle size measurements (Fig. S7).

In PP with stabilizer, particle size and MW are not affected up to 300 h of weathering. Surface abrasion however is clearly traceable in the SEM images, where rough edges disappear from being rounded off (Fig. 5B). The induction period observed here is relatively short. We expect a much longer stability if an efficient UV-stabilizer, e.g., a Hindered Amine Light Stabilizer (HALS), is added to the polymer, which is usually the case in polymers for outdoor use. Once the stabilizer combination is consumed, degradation sets in rapidly, leading to an exponential decrease in molecular weight and particle size, and a high fragmentation rate, accompanied by an increase in crystallinity and the formation of functional groups resulting from degradation. Comparing stage III for both experiments, the influence of the stabilizer becomes negligible. While it suppresses degradation for the first 300 h, polymer break-down is accelerated from 400–600 h.

The fragmentation rate of PP is extraordinarily high, and even faster for the stabilized, than for the non-stabilized fraction. This is a striking observation, indicating that the stabilizers and their degradation products accelerate fragmentation, even though they assure some stability in early stages of exposure. From one mother particle ( $\sim 190 \mu\text{m}$ ) 100,000 daughter particles are created and released within  $\sim 2$  years (3200 h accelerated weathering). Within the last stage however, the daughter particles from both experiments have almost the same size ( $\sim 5 \mu\text{m}$ ), low MW ( $M_n = 1000 \text{ g/mol}$ ), a crystallinity ( $\chi_c$ ) of 50–60%, and a similar proportion of functional groups (Fig. 1-4).

The small size of MP enables an easy distribution throughout multiple environmental compartments, ingestion by aquatic organisms and accumulation through the food chain [60]. A recent study has demonstrated, that secondary PP MP particles, especially with sizes  $< 20 \mu\text{m}$  are cytotoxic to human cells [17]. In addition to their small size, sharp edges from fragmentation [61], the degree of weathering, and accumulation of oxygen-containing functional groups [62], as well as the leaching of additives [63] may further enhance the cytotoxicity to living organisms. This highlights not only the necessity to evaluate the effects of relevant, weathered samples in future studies, but also the urge for a further evaluation of the environmental behavior and the ecological risks MP and NP particles may bear.

## Conclusion

We conclude, that the stabilizer combination present in our PP sample prevents degradation for a time frame of 300–350 h, while the non-stabilized PP starts to degrade immediately. The stability period of 350 h is very short and can be explained by the fact that the PP used in this study contains only a small amount of additives preventing thermal and photochemical oxidation.

The fragmentation rate of PP is particularly high. Comparing the time constants of particle disintegration, we estimate that PP degrades  $\sim 6$  times faster than PS [5], and  $\sim 4$  times faster than LDPE [41]. The average particle size of the reference ( $\sim 190 \mu\text{m}$ ) decreases down to  $4 \mu\text{m}$  after 3200 h of irradiation with simulated solar radiation, which is comparable to  $\sim 2$  years of outdoor weathering in Central Europe (Tab. S1). From one PP mother particle, 100,000 daughter particles are formed, and released into the environment. This value is extraordinarily high, and highlights the immense secondary PP MP-pollution from inadequate waste disposal.

The degradation of polymers under environmental conditions is a complex process, whereas laboratory experiments, like the ones presented here, can be run with reduced complexity. In our case, the simultaneous influence of solar radiation, and mechanical stress was investigated. From such experiments, a large number of samples can be collected after freely selectable time intervals, thus aged MP particles become available in sufficient amounts for detailed analysis. This allows investigations with a multitude of analytical methods, including e.g., solid-state NMR spectroscopy. Despite the reduced number of experimental parameters, we believe that the major conclusions from laboratory weathering can be transferred to environmental conditions. In this context, our experiment resembles the degradation of PP on the surface of a river or the sea, neglecting the influence of biofilms. The experimental setup, with a permanent exposure of the MP to simulated solar radiation, in combination with mechanical stress induced by stirring, provides optimum conditions for the degradation of MP. In natural environments, additional parameters control the time scales, in which degradation occurs. Exemplarily, biofilm formation may serve as a shield, and thus may lower light exposure. If biofilm formation leads to an increase of the particle density, it may even sink to the ground, where the absence of sunlight combined with a very small amount of oxygen leads to an increase of the MP-lifetime by several orders of magnitude.

It is essential to consider, that the chemical structure of the small daughter MP particles, obtained at the end of our artificial ageing experiment, is very different from the starting material. The highly weathered and fragmented secondary daughter MP particles consist of hydrocarbon chains with a molecular weight of 1000 g/mol, and a large number of oxygen-containing functional groups, e.g., carboxylic acids. Their physical properties and chemical composition have largely changed, no longer resembling pristine PP. We expect, that these particles could be much more prone to biodegradation compared to the hydrophobic, high molecular weight starting material. This question should be addressed in future studies.

#### Abbreviations

PP: Polypropylene; MP: Microplastic; PS: Polystyrene; PE: Polyethylene; HT-GPC: High temperature gel permeation chromatography; SEM: Scanning electron microscopy; DSC: Differential scanning calorimetry; MAS-NMR spectroscopy: Magic angle spinning nuclear magnetic resonance spectroscopy; FTIR spectroscopy: Fourier-transform infrared spectroscopy; Py-GC-MS: Pyrolysis gas chromatography mass spectrometry; MALDI-TOF MS: Matrix assisted laser desorption ionization-time of flight mass spectrometry; DHB: 2,5-Dihydroxybenzoic acid; THF: Tetrahydrofuran; PTFE: Polytetrafluorethylene; MW: Molecular weight; MWD: Molecular weight distribution;  $M_n$ : Number-averaged molecular weight;  $M_w$ : Weight-averaged molecular weight;  $\bar{D}$ : Dispersity; TCB: 1,2,4-Trichlorobenzene; HDPE: High density polyethylene; FESEM: Field-emission scanning electron microscopy;  $CDCl_3$ : Deuterated chloroform; HALS: Hindered amine light stabilizer.

## Supplementary Information

The online version contains supplementary material available at <https://doi.org/10.1186/s43591-022-00042-2>.

**Additional file 1: Figure S1.** Global horizontal irradiation for Europe and for Germany in kWh/m<sup>2</sup> for 2019. Source: SOLARGIS. **Figure S2.** Q-SUN daylight-Q filter compared to direct sunlight. Modified from Q-Lab Corporation, 2014, Technical Bulletin LX-5060, A Choice of Filters for Q-Sun Xenon Test Chambers. **Figure S3.** (A) MALDI spectrum of the first processing stabilizer in PP HP526 J. The three prominent peaks could be assigned to the oxidized species of Irgafos<sup>®</sup> 168 (Schwarzinger et al., 2012). (B) Chemical structure of Irgafos<sup>®</sup> 168 (Tris(2,4-di-tert-butylphenyl) phosphite) and (C) Tris(2,4-di-tert-butylphenyl)phosphate together with m/z values from the literature. **Figure S4.** (A) MALDI-TOF MS spectrum of the second processing stabilizer in PP HP526 J. The prominent peaks are identical to those arising from Irganox<sup>®</sup> 1010 reference material, treated with simulated solar radiation in THF for 100 h in (B). The structure of Irganox<sup>®</sup> 1010 is given in (C). **Figure S5.** Comparison of <sup>1</sup>H (A), <sup>13</sup>C (B), and <sup>31</sup>P (C) NMR spectra of the first extracted additive, tris(2,4-di-tert-butylphenyl)-phosphate and Irgafos<sup>®</sup> 168 as well as <sup>1</sup>H (D), <sup>13</sup>C (E) spectra of the second extracted additive, Irganox<sup>®</sup> 1010 and Irganox<sup>®</sup> 1010 reference material, treated with simulated solar radiation in THF for 100 h. The <sup>1</sup>H and <sup>13</sup>C spectra were normalised to the proton and carbon resonances of tert-butyl groups and the <sup>31</sup>P spectra to the highest peak. **Figure S6.** Above: Scheme for the photooxidative degradation of PP explaining the formation of hydroperoxides, alcohols, ketones, olefins and carboxylic acids. Below: Reactions of the radical scavenger Irgafos<sup>®</sup> 168 with reactive hydroperoxides and peroxy- and alkoxy radicals. The reactive intermediates marked in red (above) are deactivated by the phosphite Irgafos<sup>®</sup> 168 which itself is oxidized to the phosphate [51]. **Figure S7.** Average particle size distributions for (A) PP with stabilizer and (B) PP particles without stabilizer. **Figure S8.** Molecular weight distributions in g/mol of (A) PP with stabilizer and (B) PP without stabilizer for exposure time intervals from 0 h to 3200 h. **Figure S9.** DSC measurements. Heat flow in W/g vs. temperature in °C for (A) PP particles with stabilizer and (B) PP particles without stabilizer. **Figure S10.** <sup>13</sup>C CP MAS NMR spectrum of the PP particles with stabilizer prior to weathering with signal assignment. In the enlarged PP spectra (blue and orange rectangle) the differences of the resonances of the amorphous (signal a1 and b1) and crystalline (signal a2 and b2) phase become visible [52]. **Figure S11.** <sup>13</sup>C CP MAS NMR spectra of the PP particles with (A) and without (B) stabilizer for 0, 400 and 3200 h weathering time. Upon irradiation, a shift of signal intensity from the amorphous phase resonances (30 ppm, 48 ppm) to the crystalline phase resonances (28 ppm, 46 ppm) is observed [52]. The spectra are normalised to the integral of the backbone signal (35-20 ppm and 55-35 ppm). **Figure S12.** <sup>13</sup>C CP MAS NMR spectra of the PP particles with stabilizer for 0, 2800 and 3200 h weathering time. The spectra are normalised to the intensity of the methyl side chain carbon signal (at approx. 24 ppm). Individual spectra are shifted vertically for better comparability. Additionally, the baselines (green), individual refinements for the peaks (black) and the cumulative lineshape (orange) are shown in the spectra. No refinement of vinylidenes was performed between 100 – 150 ppm since the resonances of the decomposition products of Irgafos<sup>®</sup> 168 superimpose with the vinylidene resonances. **Figure S13.** SEM images of PP with stabilizer after irradiation for different time intervals. **Figure S14.** SEM images of PP without stabilizer after irradiation for different time intervals. **Table S1.** Calculation of total irradiance in the Q-SUN Xe-3 chamber. **Table S2.** Average particle sizes in µm for PP samples with and without stabilizer at exposure times from 0 h to 3200 h. Values display the average of three measurements. **Table S3.** Number-average ( $M_n$ ), weight-average ( $M_w$ ), peak ( $M_p$ ) molecular weights in g/mol, and dispersity ( $\bar{D}$ ) values for PP samples with and without stabilizer for different exposure times. **Table S4.** Crystallinity and melting temperature measurements for PP with stabilizer and PP without stabilizer. **Table S5.** Refinement parameters for the <sup>13</sup>C CP MAS NMR spectra of weathered PP samples with and without stabilizer. Refinements were carried out with pseudo-Voigt lineshapes (Eq. 1) where  $\delta_{iso}$  is the isotropic chemical shift, LB the line broadening,  $x$  the Gauss/Lorentz ratio and  $I$  the relative intensity. The latter is given in percent as fraction of the total spectral intensity. Refinement parameters

marked in grey were obtained by simultaneous free refinements of defect peaks in the two spectra with longest weathering times and were kept constant in the subsequent refinements. **Table S6.** Correction factors for PP with and without stabilizer determined with quantitative multi-CP spectra of the respective 3200 h weathered sample. Used to calibrate the defect intensities in the CP spectra [5].

### Acknowledgements

The authors would like to thank Lisa Weber, Martina Fried and Dr. Daniel Wagner for particle preparation, Dr. Winfried Kretschmer for HT GPC analysis, Martina Heider and Dr. Ulrich Mansfeld for SEM measurements, and Dr. Francesco Rodella, Irene Bauer, Sandra Opel and Jutta Failner for help and advice concerning Soxhlet extraction and stabilizer processing.

### Authors' contributions

N.M. performed accelerated weathering of particles, particle size analysis, GPC, and DSC measurements. A.M. performed solid-state and liquid-state NMR spectroscopic measurements. N.M. and A.M. wrote the first draft of the manuscript, T.M., H.R., V.A., P.S., and J.S. supported the discussion and finalization of the manuscript. All authors read and approved the final version of the manuscript.

### Funding

Open Access funding enabled and organized by Projekt DEAL. This project was funded by the Deutsche Forschungsgemeinschaft (DFG, German Research Foundation)—Project Number 391977956—SFB 1357, subproject C01.

### Availability of data and materials

All data needed to evaluate the conclusions in the paper are present in the paper and/or in the Supplementary Material.

### Declarations

#### Ethics approval and consent to participate

Not applicable.

#### Consent for publication

Not applicable.

#### Competing interests

The authors declare to have no competing financial or personal interests.

#### Author details

<sup>1</sup>Department of Macromolecular Chemistry I, University of Bayreuth, Universitätsstraße 30, 95447 Bayreuth, Germany. <sup>2</sup>Department of Inorganic Chemistry III and Northern Bavarian NMR Centre, University of Bayreuth, Universitätsstraße 30, 95447 Bayreuth, Germany. <sup>3</sup>Department of Polymer Engineering, University of Bayreuth, Universitätsstraße 30, 95447 Bayreuth, Germany.

Received: 1 July 2022 Accepted: 7 September 2022

Published online: 21 September 2022

### References

- PlasticsEurope. *Plastics - The Facts 2020: An analysis of European plastics production, demand and waste data*; 2020.
- Bishop G, Styles D, Lens PNL. Recycling of European plastic is a pathway for plastic debris in the ocean. *Environ Int.* 2020;142: 105893.
- Chen HL, Nath TK, Chong S, Foo V, Gibbins C, Lechner AM. The plastic waste problem in Malaysia: management, recycling and disposal of local and global plastic waste. *SN Applied Sciences.* 2021;3(4):1–15.
- Andrady AL. Microplastics in the marine environment. *Mar Pollut Bull.* 2011;62(8):1596–605.
- Meides N, Menzel T, Poetzschner B, Löder MGJ, Mansfeld U, Stroehriegl P, et al. Reconstructing the Environmental Degradation of Polystyrene by Accelerated Weathering. *Environ Sci Technol.* 2021;55(12):7930–8.
- Hartmann NB, Hüffer T, Thompson RC, Hassellöv M, Verschoor A, Daugaard AE, et al. Are we speaking the same language? Recommendations for a definition and categorization framework for plastic debris. *Environ Sci Technol.* 2019;53(3):1039–47.
- Andrady AL. The plastic in microplastics: A review. *Mar Pollut Bull.* 2017;119(1):12–22.
- Wu X, Liu P, Shi H, Wang H, Huang H, Shi Y, et al. Photo aging and fragmentation of polypropylene food packaging materials in artificial seawater. *Water Research.* 2021;188:116456.
- Duan J, Bolan N, Li Y, Ding S, Atugoda T, Vithanage M, et al. Weathering of microplastics and interaction with other coexisting constituents in terrestrial and aquatic environments. *Water Research.* 2021;196:117011.
- Kumar M, Xiong X, He M, Tsang DCW, Gupta J, Khan E, et al. Microplastics as pollutants in agricultural soils. *Environ Pollut.* 2020;265(Pt A): 114980.
- Gewert B, Plassmann MM, MacLeod M. Pathways for degradation of plastic polymers floating in the marine environment. *Environ Sci Process Impacts.* 2015;17(9):1513–21.
- Zweifel H. Principles of oxidative degradation. In: *Stabilization of Polymeric Materials.* Springer; 1998. p. 1–40.
- Kirstein IV, Kirmizi S, Wichels A, Garin-Fernandez A, Erler R, Löder M et al. Dangerous hitchhikers? Evidence for potentially pathogenic *Vibrio* spp. on microplastic particles. *Marine Environmental Research* 2016; 120:1–8. Available from: URL: <https://www.sciencedirect.com/science/article/pii/S01411361630112X>.
- Zettler ER, Mincer TJ, Amaral-Zettler LA. Life in the “Plastisphere”: Microbial Communities on Plastic Marine Debris. *Environ Sci Technol.* 2013;47(13):7137–46.
- Imhof HK, Ivleva NP, Schmid J, Niessner R, Laforsch C. Contamination of beach sediments of a subalpine lake with microplastic particles. *Curr Biol.* 2013;23(19):R867–8.
- Imhof HK, Rusek J, Thiel M, Wolinska J, Laforsch C. Do microplastic particles affect *Daphnia magna* at the morphological, life history and molecular level? *PLoS ONE.* 2017;12(11): e0187590.
- Hwang J, Choi D, Han S, Choi J, Hong J. An assessment of the toxicity of polypropylene microplastics in human derived cells. *Sci Total Environ.* 2019;684:657–69.
- Engler RE. The Complex Interaction between Marine Debris and Toxic Chemicals in the Ocean. *Environ Sci Technol.* 2012;46(22):12302–15.
- Avio CG, Gorb S, Regoli F. Plastics and microplastics in the oceans: From emerging pollutants to emerged threat. *Mar Environ Res.* 2017;128:2–11.
- Barrick A, Champeau O, Chatel A, Manier N, Northcott G, Tremblay LA. Plastic additives: challenges in ecotox hazard assessment. *PeerJ.* 2021;9: e11300.
- OECD. Considerations and criteria for sustainable plastics from a chemicals perspective (Background Paper 1): OECD Global Forum on Environment: Plastics in a Circular Economy Designing Sustainable Plastics from a Chemicals Perspective. [OECD Environment, Health and Safety Publications, Series on Risk Management]. No. 53; 2018. Available from: URL: <https://www.oecd.org/chemicalsafety/risk-management/considerations-and-criteria-for-sustainable-plastics-from-a-chemicals-perspective.pdf>.
- Blázquez-Blázquez E, Cerrada ML, Benavente R, Pérez E. Identification of Additives in Polypropylene and Their Degradation under Solar Exposure Studied by Gas Chromatography-Mass Spectrometry. *ACS Omega.* 2020;5(16):9055–63.
- Biale G, La Nasa J, Mattonai M, Corti A, Vinciguerra V, Castelvetro V, et al. A systematic study on the degradation products generated from artificially aged microplastics. *Polymers.* 2021;13(12):1997.
- Garvey CJ, Impéror-Clerc M, Rouzière S, Gouadec G, Boyron O, Rowenczyk L, et al. Molecular-Scale Understanding of the Embrittlement in Polyethylene Ocean Debris. *Environ Sci Technol.* 2020;54(18):11173–81.
- Shi Y, Qin J, Tao Y, Jie G, Wang J. Natural weathering severity of typical coastal environment on polystyrene: Experiment and modeling. *Polym Testing.* 2019;76:138–45.
- Gewert B, Plassmann M, Sandblom O, MacLeod M. Identification of chain scission products released to water by plastic exposed to ultraviolet light. *Environ Sci Technol Lett.* 2018;5(5):272–6.

27. Grause G, Chien M-F, Inoue C. Changes during the weathering of polyolefins. *Polymer degradation and stability* 2020:109364.
28. Da Costa JP, Nunes AR, Santos PSM, Giraó AV, Duarte AC, Rocha-Santos T. Degradation of polyethylene microplastics in seawater: Insights into the environmental degradation of polymers. *Journal of Environmental Science and Health, Part A*. 2018;53(9):866–75.
29. Ojeda T, Freitas A, Birck K, Dalmolin E, Jacques R, Bento F, et al. Degradability of linear polyolefins under natural weathering. *Polym Degrad Stab*. 2011;96(4):703–7.
30. Khelassi A, Belhaneche-Bensemra N. Investigation of pro-oxidant agents' effects on the ageing of polypropylene bags. *Int J Environ Stud*. 2020;77(2):264–74.
31. Brandon J, Goldstein M, Ohman MD. Long-term aging and degradation of microplastic particles: Comparing in situ oceanic and experimental weathering patterns. *Mar Pollut Bull*. 2016;110(1):299–308.
32. Andradý AL, Koongolla B. Degradation and Fragmentation of Microplastics. In: *Plastics and the Ocean*. John Wiley & Sons, Ltd; 2022. p. 227–68.
33. Efimova I, Bagaeva M, Bagaev A, Kileso A, Chubarenko IP. Secondary Microplastics Generation in the Sea Swash Zone With Coarse Bottom Sediments: Laboratory Experiments. *Front Mar Sci*. 2018;5:313.
34. Al-Malaika S. Oxidative degradation and stabilisation of polymers. *Int Mater Rev*. 2003;48(3):165–85.
35. Carlsson DJ, Wiles DM. The Photooxidative Degradation of Polypropylene. Part I. Photooxidation and Photoinitiation Processes. *Journal of Macromolecular Science, Part C: Polymer Reviews* 1976; 14(1):65–106.
36. Allen NS, Chirinos-Padron A, Henman TJ. Photoinitiated oxidation of polypropylene: a review. *Prog Org Coat*. 1985;13(2):97–122.
37. Kalogerakis N, Karkanorachaki K, Kalogerakis GC, Triantafyllidi EI, Gotsis AD, Partisinelos P et al. Microplastics Generation: Onset of Fragmentation of Polyethylene Films in Marine Environment Mesocosms. *Frontiers in Marine Science* 2017; 4. Available from: URL: <https://www.frontiersin.org/article/https://doi.org/10.3389/fmars.2017.00084>.
38. Julienne F, Delorme N, Lagarde F. From macroplastics to microplastics: Role of water in the fragmentation of polyethylene. *Chemosphere*. 2019;236: 124409.
39. Mattsson K, Björkroth F, Karlsson T, Hassellöv M. Nanofragmentation of Expanded Polystyrene Under Simulated Environmental Weathering (Thermo-oxidative Degradation and Hydrodynamic Turbulence). *Front Mar Sci*. 2021;7:1252.
40. Born MP, Brüll C. From model to nature - A review on the transferability of marine (micro-) plastic fragmentation studies. *Sci Total Environ*. 2022;811: 151389.
41. Menzel T, Meides N, Mauer A, Mansfeld U, Kretschmer W, Kuhn M, et al. Degradation of low-density polyethylene to nanoplastic particles by accelerated weathering. *Sci Total Environ*. 2022;826:154035.
42. Johnson RL, Schmidt-Rohr K. Quantitative solid-state <sup>13</sup>C NMR with signal enhancement by multiple cross polarization. *J Magn Reson*. 2014;239:44–9.
43. Mauer A, Pötzschner B, Meides N, Siegel R, Strohriegel P, Senker J. Quantification of photooxidative defects in weathered microplastics using <sup>13</sup>C multiCP NMR spectroscopy. *RSC Adv*. 2022;12(18):10875–85.
44. Canopoli L, Coulon F, Wagland ST. Degradation of excavated polyethylene and polypropylene waste from landfill. *Sci Total Environ*. 2020;698: 134125.
45. Dong M, Zhang Q, Xing X, Chen W, She Z, Luo Z. Raman spectra and surface changes of microplastics weathered under natural environments. *Sci Total Environ*. 2020;739: 139990.
46. Fernández-González V, Andrade-Garda JM, López-Mahía P, Muniategui-Lorenzo S. Impact of weathering on the chemical identification of microplastics from usual packaging polymers in the marine environment. *Anal Chim Acta*. 2021;1142:179–88.
47. Veeman WS. Carbon-13 chemical shift anisotropy. *Prog Nucl Magn Reson Spectrosc*. 1984;16:193–235.
48. Schwarzinger C, Gabriel S, Reißmann S, Buchberger W. Quantitative Analysis of Polymer Additives with MALDI-TOF MS Using an Internal Standard Approach. *J Am Soc Mass Spectrom*. 2012;23(6):1120–5.
49. Fouyer K, Lavastre O, Rondeau D. Direct monitoring of the role played by a stabilizer in a solid sample of polymer using direct analysis in real time mass spectrometry: the case of Irgafos 168 in polyethylene. *Anal Chem*. 2012;84(20):8642–9.
50. BASF. Safety Data Sheet Irgafos 168 FF; 2017 [cited 2017 Aug 2]. Available from: URL: <https://basf.available-equipment.com/ProductDocument.aspx?ID=195&type=11>.
51. Maier R-D, Schiller M. *Handbuch Kunststoff Additive*. Carl Hanser Verlag GmbH Co KG; 2016.
52. Hronský V, Koval'áková M, Vrábel P, Uhrínová M, Olčák D. Estimation of the Degree of Crystallinity of Partially Crystalline Polypropylenes Using <sup>13</sup>C NMR. *Acta Physica Polonica, A* 2014; 125(6).
53. Ehrenstein G. *Polymer-Werkstoffe: Struktur-Eigenschaften-Anwendung*; 1999.
54. Li J, Yang R, Yu J, Liu Y. Natural photo-aging degradation of polypropylene nanocomposites. *Polym Degrad Stab*. 2008;93(1):84–9.
55. Craig IH, White JR, Kin PC. Crystallization and chemi-crystallization of recycled photo-degraded polypropylene. *Polymer*. 2005;46(2):505–12.
56. Mowery DM, Assink RA, Derzon DK, Klamo SB, Clough RL, Bernstein R. Solid-state <sup>13</sup>C NMR investigation of the oxidative degradation of selectively labeled polypropylene by thermal aging and  $\gamma$ -irradiation. *Macromolecules*. 2005;38(12):5035–46.
57. Mowery DM, Clough RL, Assink RA. Identification of oxidation products in selectively labeled polypropylene with solid-state <sup>13</sup>C NMR techniques. *Macromolecules*. 2007;40(10):3615–23.
58. Wool RP. Self-healing materials: a review. *Soft Matter*. 2008;4(3):400–18.
59. Rajakumar K, Sarasvathy V, Thamarai Chelvan A, Chitra R, Vijayakumar CT. Natural Weathering Studies of Polypropylene. *J Polym Environ*. 2009;17(3):191.
60. Xu C, Zhang B, Gu C, Shen C, Yin S, Amir M et al. Are we underestimating the sources of microplastic pollution in terrestrial environment? *Journal of Hazardous Materials* 2020:123228.
61. Völkl M, Jérôme V, Weig A, Jasinski J, Meides N, Strohriegel P, et al. Pristine and artificially-aged polystyrene microplastic particles differ in regard to cellular response. *J Hazard Mater*. 2022;435: 128955.
62. Yu X, Lang M, Huang D, Yang C, Ouyang Z, Guo X. Photo-transformation of microplastics and its toxicity to Caco-2 cells. *Sci Total Environ*. 2022;806:150954.
63. Bridson JH, Gaugler EC, Smith DA, Northcott GL, Gaw S. Leaching and extraction of additives from plastic pollution to inform environmental risk: A multidisciplinary review of analytical approaches. *Journal of Hazardous Materials* 2021; 414:125571. Available from: <https://www.sciencedirect.com/science/article/pii/S0304389421005343>.

Submit your manuscript to a SpringerOpen<sup>®</sup> journal and benefit from:

- Convenient online submission
- Rigorous peer review
- Open access: articles freely available online
- High visibility within the field
- Retaining the copyright to your article

---

Submit your next manuscript at ► [springeropen.com](https://www.springeropen.com)

---